ACS Energy LETTERS

http://pubs.acs.org/journal/aelccp

Monolithic Perovskite Solar Capacitor Enabled by Double-Sided TiO_2 Nanotube Arrays

Meng Zhang and Zhiqun Lin*

Cite This: *ACS Energy Lett.* 2022, 7, 1260−1265

Read Online

ACCESS | Metrics & More | Article Recommendations | Supporting Information

ABSTRACT: An integrated power pack that renders simultaneous solar energy harvesting and storage represents a particularly promising energy source toward future applications. Herein, we report a high-performance hybrid power pack of perovskite solar cell (PSC) and supercapacitor via capitalizing on double-sided TiO_2 nanotube arrays that have a dual-function as electron transport layer (ETL) for PSC and cathode for supercapacitor, respectively (i.e., a monolithic perovskite solar capacitor). Specifically, a simple yet robust acid-treatment strategy followed by selective oxygen plasma exposure on only the PSC side is employed to concurrently increase the performance of double-sided TiO_2 nanotube electrodes in both the PSC and supercapacitor units. Intriguingly, the integrated power pack delivers fast response under photocharging because of efficient charge transfer across the two sides of the TiO_2 nanotube array electrode, attaining a high overall optoelectrical energy conversion and storage efficiency of 9.18%. This work demonstrates a viable route to engineering intimately linked energy conversion−storage systems of interest.

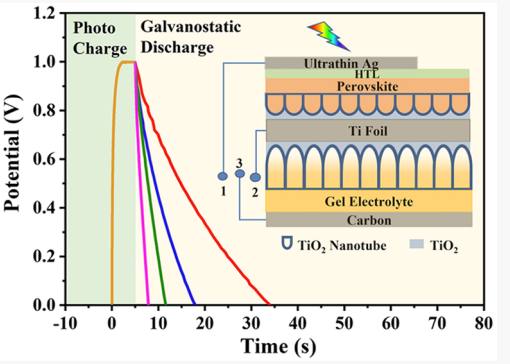

An integrated solar power pack, imparting both solar energy conversion and electric storage in one device, affords an efficient platform to mitigate the power output swing resulting from light intensity fluctuation and diurnal cycles. Notably, supercapacitors are the most widely adopted energy storage device incorporated with solar cells owing to their high power density, fast charge−discharge rate, long cycling life, and good operational safety.[1] However, previous attempts to stack solar cells (often dye-sensitized solar cells and organic solar cells) with supercapacitors suffer from low charging voltage and low energy density due primarily to the inferior performance of the former.[1,2] Recently, perovskite solar cells (PSCs) have rapidly emerged as extremely promising next-generation photovoltaics because of the outstanding optoelectronic properties of metal halide perovskites, including large absorption coefficient, high ambipolar carrier mobility, long carrier diffusion length, and inherent tolerance to defects.[3−6] Remarkably, the power conversion efficiency (PCE) of PSCs has skyrocketed to 25.5%,[7] positioning them as notable candidates to recharge supercapacitors via harvesting solar energy.

Integration of a solar cell and supercapacitor can be implemented via either independently connecting an operational solar cell and a supercapacitor through an external circuit[8,9] or combining the solar cell and supercapacitor into a monolithic device via a shared electrode. However, the former method of integration results in large additional Ohmic loss, high cost, and lack of dynamic solar light control. To this end, efforts have been centered on intimately combining the PSC and supercapacitor into a single device. Notably, effective routes to rendering monolithic devices have been comparatively few and limited in scope, within which a shared carbon electrode is often employed because carbon materials have been widely used as electrodes in both PSCs and supercapacitors.[10−14] Nonetheless, solid-state supercapacitors and thick carbon-based electrodes are often required in order to prevent the decomposition of PSCs because of the ionic crystal nature of perovskites when exposed to humidity, UV light, polar solvents, etc. Undoubtedly, the instability of perovskites, and thus the poor long-term stability of the resulting PSCs, imposes many obstacles in producing a single, closely connected PSC−supercapacitor device. As such, it remains challenging to rationally design such one-piece, integrated devices that concurrently balance efficiency, long-term stability, fabrication flexibility and compatibility, and compactness.

Herein, we report a high-performance power stack realized via integrating a PSC and a supercapacitor rendered by

Received: January 12, 2022
Accepted: March 4, 2022
Published: March 7, 2022

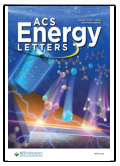

https://doi.org/10.1021/acsenergylett.2c00090
ACS Energy Lett. 2022, 7, 1260−1265

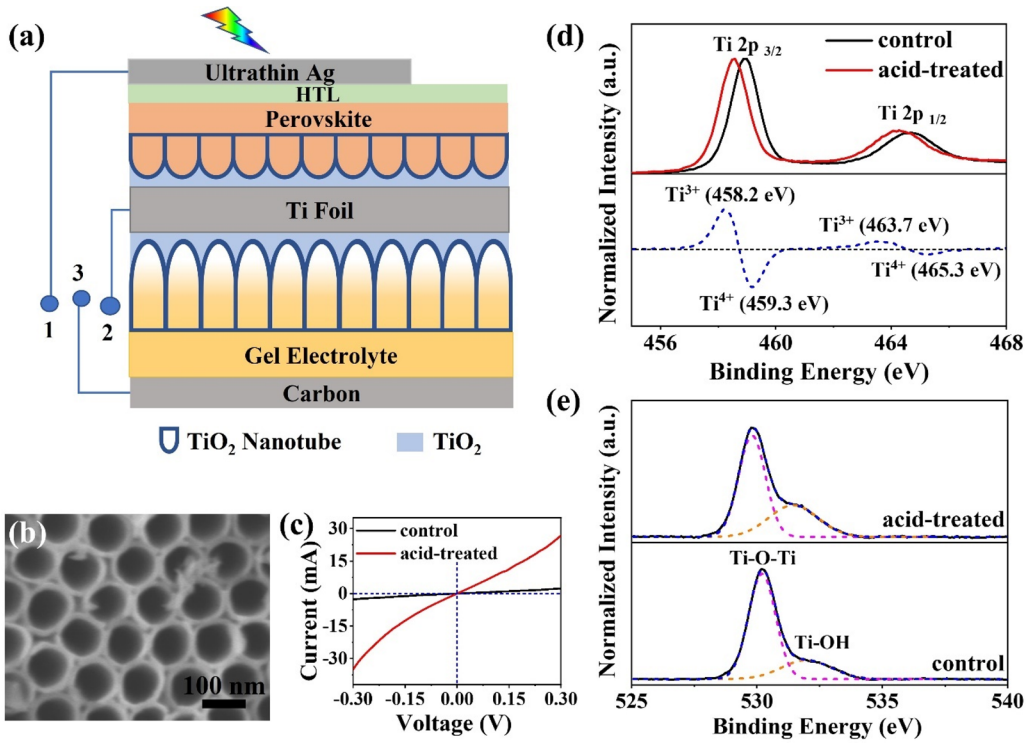

Figure 1. (a) Schematic of monolithic perovskite solar capacitor (i.e., hybrid power pack composed of PSC and supercapacitor) rendered by double-sided TiO_2 nanotube array electrode formed via anodization of Ti foil. (b) Representative SEM image of TiO_2 nanotube after acid treatment. (c) Linear sweep voltammetry curves of TiO_2 nanotube array film with and without (control sample) acid treatment. (d) Normalized Ti 2p XPS spectra of TiO_2 nanotubes with and without acid treatment (upper panel). Their spectral difference is shown in the lower panel. (e) Normalized O 1s XPS spectra of TiO_2 nanotube with and without acid treatment.

capitalizing on double-sided TiO_2 nanotube arrays as the electrode. The direct growth of TiO_2 nanotube arrays on both sides of a highly conductive Ti foil not only ensures efficient charge transfer between the PSC and supercapacitor but also allows for a robust chemical barrier for the fabrication of the PSC, thereby greatly impacting the flexibility in processing the supercapacitor. A simple acid treatment to the TiO_2 nanotube array electrode, followed by selective oxygen plasma exposure on the PSC subcell, is found to simultaneously improve the performance of both PSC and supercapacitor. Taking advantage of the optimized PSC and supercapacitor, the integrated device achieves an enhanced overall optoelectrical energy conversion and storage efficiency of 9.18% with fast response and superior cycling capability.

Design of Integrated Power Pack. Figure 1a depicts the configuration of the integrated device. Specifically, two TiO_2 nanotube arrays grown on the two sides of a Ti foil via electrochemical anodization are employed as electrode. The upper configuration illustrates the PSC fabricated with TiO_2 nanotube arrays that function as the ETL and scaffold for perovskite deposition. The lower configuration outlines the TiO_2 nanotube array-based asymmetric supercapacitor for storing electricity generated by the PSC. Because of the excellent conductivity of the Ti foil, electrons could be easily transferred between the two separated TiO_2 nanotube array electrodes bridged by the Ti foil, thus enabling the photocharging or discharging of the supercapacitor. It is particularly noteworthy that the Ti foil, as a robust partition, renders the fabrication of the PSC and supercapacitor relatively independent, and more importantly, it protects the perovskite from any possible damage caused during the processing and operation of the supercapacitor.

It is notable that pristine TiO_2 nanotube arrays produced via anodization of Ti foil (see Experimental Section in the Supporting Information) displayed very low specific capacitance because of its low conductivity as a result of its semiconductor characteristics.[15,16] Hydrogenation via hydrogen thermal treatment, hydrogen plasma, or electrochemical reduction has been proven to be an effective means of improving the conductivity of TiO_2 via introducing oxygen vacancies and forming Ti^{3+} state for supercapacitor applications.[17] Similarly, simple acid treatment has also been developed in our previous work to create oxygen vacancies in TiO_2 for efficient charge transport in PSCs.[18] Compared to the hydrogenation routes noted above, acid treatment does not involve rigorous heating or extra instruments and is facile and controllable. Thus, the acid-treatment strategy was implemented in this work to render superior performance of TiO_2 nanotube arrays for both PSC and supercapacitor subcells in hybrid power stack. Notably, no obvious morphology change of TiO_2 nanotubes after acid treatment (diameter, $D \approx 100$ nm; wall thickness, $t \approx 10$ nm; Figure 1b). The formation of oxygen vacancies and Ti^{3+} states in TiO_2 nanotubes after acid treatment was examined by X-ray photoelectron spectroscopy (XPS) (Figure 1d). Specifically, the subtraction in the Ti 2p spectra of acid-treated TiO_2 with respect to control sample displays the characteristic Ti $2p_{3/2}$ (458.2 eV) and Ti $2p_{1/2}$ (463.7 eV) peaks of Ti^{3+}.[19] In addition, increased hydroxyl groups were observed in the XPS spectra of O 1s on acid-treated TiO_2 nanotubes (Figure 1e), which can be ascribed to the reaction between adsorbed H_2O and TiO_2 (H_2O + Ti−O−

https://doi.org/10.1021/acsenergylett.2c00090
ACS Energy Lett. 2022, 7, 1260−1265

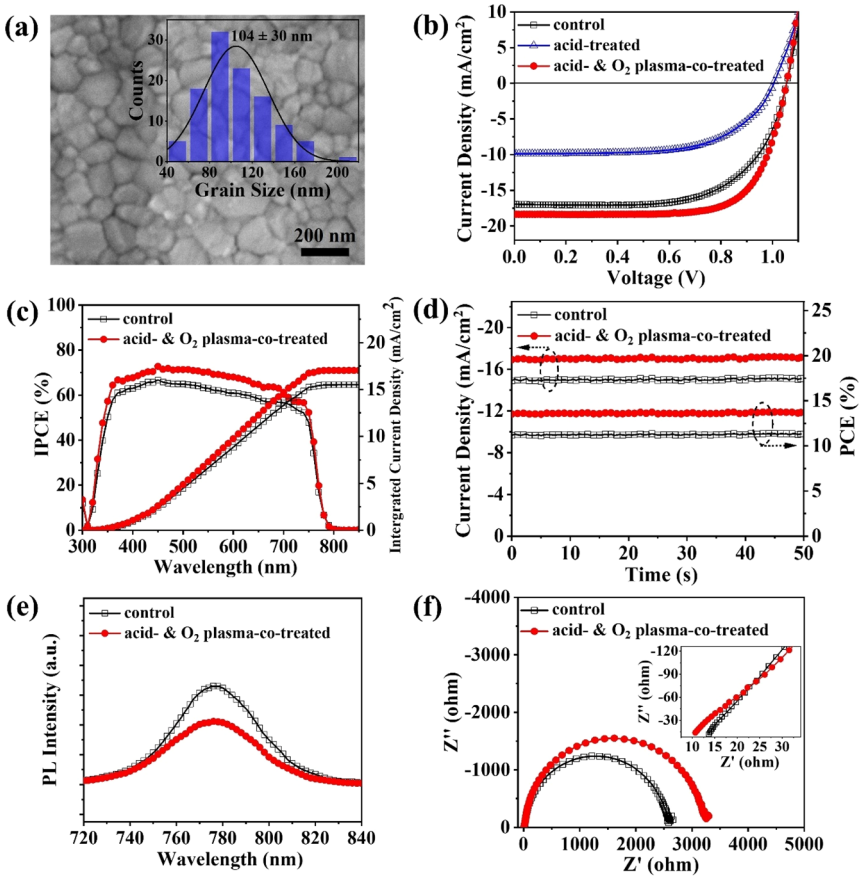

Figure 2. (a) Representative SEM image of perovskite absorber over the surface of TiO_2 nanotube ETL after acid and oxygen plasma treatments. The inset shows the corresponding grain size distribution. (b) $J-V$ curves of champion PSCs undergoing different treatments on TiO_2 nanotube ETL. (c) IPCE spectra, (d) stable J_{SC} and PCE, (e) PL spectra, and (f) Nyquist plots of electrochemical impedance spectroscopy of PSCs with and without (control sample) acid and oxygen plasma treatments on TiO_2 nanotube ETL.

Ti → 2Ti−OH).[20] Both emerged oxygen vacancies and increased surface hydroxyl contents in TiO_2 have been reported to greatly enhance its capacitance performance.[19] Thus, it is not surprising that the conductivity of TiO_2 nanotube arrays was markedly increased by 1 order of magnitude after acid treatment (Figure 1c), which in turn resulted in superior performance in both PSC and supercapacitor as discussed below.

PSC Employing TiO_2 Nanotube Arrays as ETL. The PSC fabricated on TiO_2 nanotubes has the configuration of Ti foil/TiO_2 nanotube arrays/perovskite/poly[bis(4-phenyl)-(2,4,6-trimethylphenyl) amine] (PTAA)/ultrathin Ag (see Experimental Section; Figure 1a). The mixed-cation and mixed-halide perovskite of $Cs_{0.05}MA_{0.16}FA_{0.79}Pb(I_{0.83}Br_{0.17})_3$ was chosen as the light absorber because of its good performance and stability.[4] An ultrathin Ag layer of 8 nm with an average transmittance of approximately 70% in the range of 400−800 nm (Figure S1a) was applied as the transparent electrode. To increase the moisture and processing stability, the PSC was encapsulated with a 5 μm thick hydrophobic parylene film via vacuum deposition. Notably, parylene has a high transmittance (~90%) over a broad range of 300−1000 nm (Figure S1b). It is worth noting that acid-treated TiO_2 nanotube arrays were treated with O_2 plasma prior to the deposition of perovskite according to our previous work.[18] This is because both surface and bulk oxygen vacancies were generated in acid-treated TiO_2 nanotubes. The bulk oxygen vacancies increase the donor density and bulk conductivity of TiO_2; the surface vacancies, however, function as the traps to trigger charge recombination when employed as ETL in PSC.[18] Thus, O_2 plasma exposure was performed to remove the surface oxygen vacancies yet retain the bulk vacancies in TiO_2 nanotube ETL for efficient charge transfer (Figure S2). It is worth noting that O_2 plasma also plays two additional roles in this work, that is, facilitating the infiltration of perovskite precursor solution into TiO_2 nanotubes and eliminating the Cl residual from acid-treatment,[18] where the latter rules out possible Cl passivation to perovskite.

As TiO_2 nanotube arrays serve as an electron collector as well as a scaffold for perovskite deposition in the PSC subcell of the hybrid power pack, their length would greatly affect the perovskite morphology and device efficiency. In this context, the length of TiO_2 nanotubes was first optimized to be 400 nm in this work (Figure S3a). As shown in Figure 2a, the perovskite absorber deposited on TiO_2 nanotubes has an average grain size of 104 nm, which is nearly equal to D of TiO_2 nanotube (~100 nm, Figure 1b), indicating the significant role of TiO_2 nanotubes in assisting perovskite growth. Figure 2b depicts the $J-V$ curves of PSCs using TiO_2 nanotubes as ETL with different treatments. As expected, the champion device with acid treatment followed by O_2 plasma exposure of TiO_2 nanotubes yielded the highest PCE of 13.98% with a short circuit current, J_{sc}, of 18.37 mA/cm^2; an open circuit voltage, V_{oc}, of 1.05 V; and a fill factor, FF, of 72.38%, as a direct consequence of suppressed photogenerated electron−hole recombination (compared to the device with

https://doi.org/10.1021/acsenergylett.2c00090
ACS Energy Lett. 2022, 7, 1260−1265

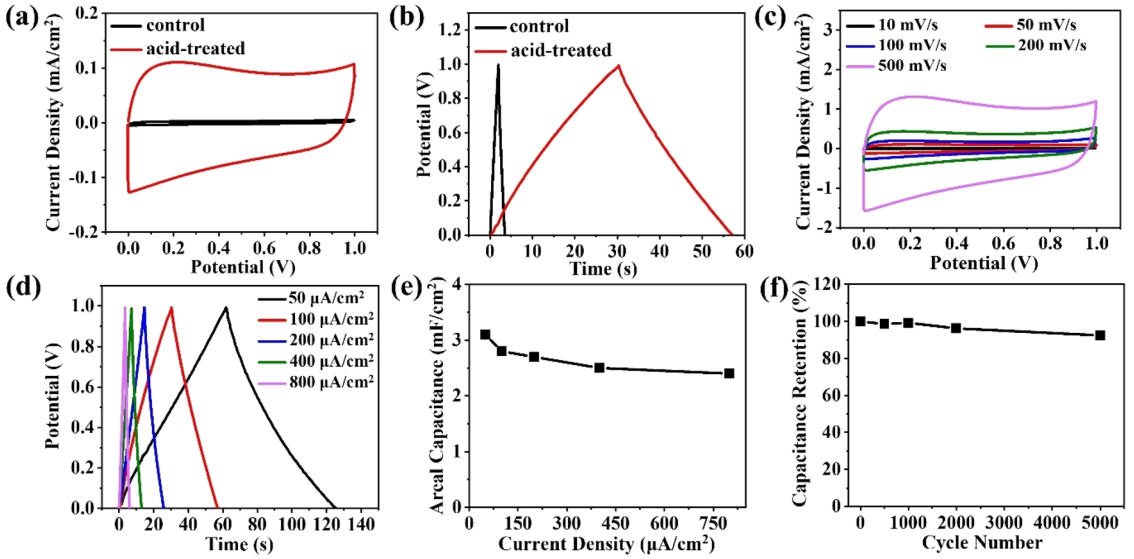

Figure 3. (a) CV curves at the scan rate of 50 mV/s and (b) galvanostatic charge/discharge curves at the current density of 100 μA/cm^2 of supercapacitors with pristine (control sample) and acid-treated TiO_2 nanotubes as electrodes. (c) CV curves at various scan rates (i.e., from 10 to 500 mV/s) and (d) galvanostatic charge/discharge curves at various current densities (i.e., from 50 to 800 μA/cm^2) of supercapacitor fabricated using acid-treated TiO_2 nanotube electrode. (e) Areal capacitance of supercapacitor with acid-treated TiO_2 nanotube electrode calculated from (d) as a function of current density. (f) Capacitance stability of supercapacitor with acid-treated TiO_2 nanotube electrode measured by the galvanostatic charge/discharge test at a scan rate of 100 mV/s for 5000 cycles.

acid treatment only) and enhanced bulk conductivity owing to the presence of bulk oxygen vacancies (in comparison to the control device). The average PCE, extracted from the $J-V$ curves of 9 independent devices, increased by 20%, that is, from 11.16 ± 0.34% for control devices to 13.43 ± 0.23% for acid- and O_2 plasma-*co*-treated devices (Figure S4). The stable output power was measured to be 11.37% and 13.62% for the control device and acid- and O_2 plasma-*co*-treated device, respectively (Figure 2d). A notable improvement over the entire wavelength range in the incident-photon-to-current conversion efficiency (IPCE) spectra was seen for the acid- and O_2 plasma-*co*-treated device over the control device (Figure 2c), signifying a lower recombination loss. The decreased recombination loss originated from a more efficient electron transfer of the TiO_2 nanotube ETL after acid and O_2 plasma treatments, as verified by the PL spectra (Figure 2e). Accordingly, a larger recombination resistance and a smaller serial resistance were seen for the acid- and O_2 plasma-*co*-treated device from the Nyquist plots of electrochemical impedance spectroscopy of PSCs (Figures 2f and S5).

Asymmetric Supercapacitor Based on TiO_2 Nanotube Electrode. Different from that in the PSC subcell, the acid-treated TiO_2 nanotube arrays do not require oxygen plasma treatment to remove surface oxygen vacancies for fabricating the supercapacitor subcell of the hybrid power pack. This is because the separation and transfer of photogenerated charge carriers in solar cells are driven by the device's built-in potential, while the charge transport in the supercapacitor is governed by an external field which could effectively eliminate the unexpected recombination owing to traps imposed by surface oxygen vacancies. To improve the capacitive performance of the TiO_2 nanotube array electrode, its length was greatly increased to 4 μm (via a two-step anodization, see Experimental Section; Figure S6) in this subcell compared to that in the PSC subcell (~400 nm; via the second anodization, see Experimental Section; Figure S3a). The capacitive performance of the as-prepared TiO_2 nanotube electrode was investigated in an asymmetric two-electrode configuration with carbon as counter electrode and poly(vinyl alcohol) (PVA):LiCl aqueous gel as electrolyte, respectively (see Experimental Section for detailed supercapacitor fabrication). As shown in Figure 3a, acid treatment did not alter the rectangular shape of the cyclic voltammogram (CV) of the corresponding supercapacitor, indicating an electric double-layer-based capacitive response. In sharp contrast to the control sample (pristine TiO_2), acid-treated TiO_2 demonstrated greatly increased charge storage capacity due to the presence of a large amount of oxygen-Ti^{3+} vacancies that served as active sites and resulted in enhanced conductivity of the TiO_2 nanotube electrode.[19,21,22] The areal capacitance of the device, evaluated by galvanostatic charge/discharge test at a current density of 100 μA/cm^2 (Figure 3b), was calculated to be 0.18 and 2.8 mF/cm^2 for the control sample and acid-treated TiO_2 nanotube-based supercapacitors, respectively, demonstrating a 16-fold increase of the latter.

The CV curves of the supercapacitor with acid-treated TiO_2 nanotubes obtained at various scan rates are shown in Figure 3c. The shapes of the CV curves remain unchanged as the scan rate increase from 10 to 500 mV/s, signifying the high-rate capability of the device. Galvanostatic charge/discharge curves were also collected for the acid-treated TiO_2 nanotube array-based supercapacitor at various current densities (Figure 3d). The areal capacitances derived from the discharge curves manifested only ~20% loss in the device capacitance (Figure 3e) when the discharge current density increased up to 16 times (from 50 to 800 μA/cm^2), suggesting a good rate capability, which is in good accordance with the CV measurements. The resulting areal energy density and power density of the devices were also calculated and are summarized in Figure S7. A good cycling stability of the acid-treated TiO_2 nanotube array-based supercapacitor was also observed with 92% retention of the initial capacitance after 5000 cycles (Figure 3f).

https://doi.org/10.1021/acsenergylett.2c00090
ACS Energy Lett. 2022, 7, 1260−1265

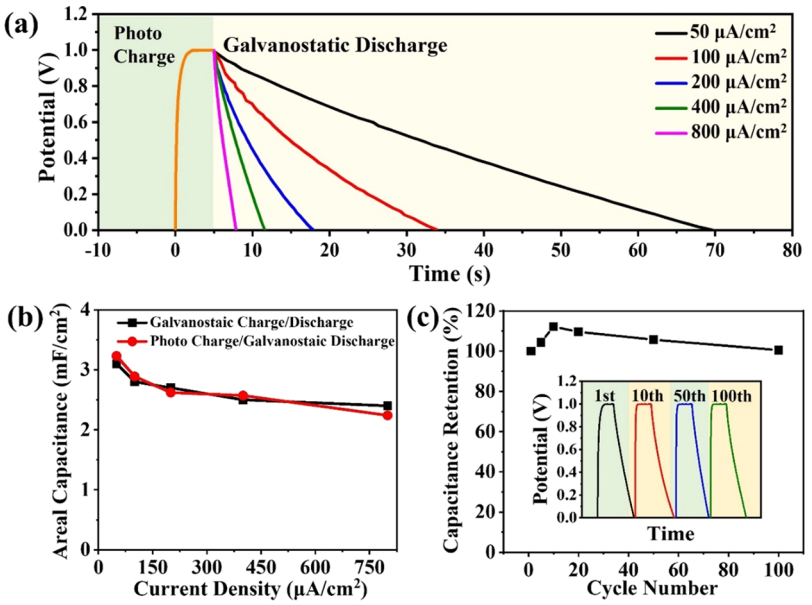

Figure 4. (a) Photo charge/galvanostatic discharge curves at various discharging current density, ranging from 50 of 800 μA/cm^2. (b) Areal capacitance of supercapacitor calculated from discharge curves under galvanostatic charge (Figure 3e) and photo charge. (c) Photo charge/galvanostatic discharge cycling stability of the integrated device (inset: photo charge/galvanostatic discharge curves of 1st, 10th, 50th, and 100th cycles).

Integrated Power Pack of PSC and Supercapacitor. After the performance of the respective subcell was optimized, an integrated device composed of PSC and supercapacitor bridged by double-sided TiO_2 nanotube on Ti foil was produced. The strategy for growing TiO_2 nanotubes with different lengths on the two sides of a Ti foil can be found in the Supporting Information (Experimental Section). On the basis of the results discussed above, acid treatment to TiO_2 nanotube electrode to both PSC and supercapacitor subcells, followed by selective oxygen plasma on the PSC subcell only, were carried out to concurrently improve the performances of the two subcells. The performance of such a hybrid power pack was evaluated in a photo charge/galvanostatic discharge mode. During the photo charge process (i.e., electrodes 1 and 3 are connected; Figure 1a), the photoexcited charges generated in the perovskite absorber were collected by the TiO_2 nanotube ETL and then directly transferred to the TiO_2 electrode of the other side through Ti foil to charge the supercapacitor. For the subsequent galvanostatic discharge process, electrodes 2 and 3 in Figure 1a were connected. It is worth noting that the voltage window of the supercapacitor and the V_{oc} of PSC in this work are highly matched, thereby facilitating energy storage and improving the performance of the resulting power pack.

Figure 4a depicts the photo charge and galvanostatic discharge processes of the integrated PSC−supercapacitor device at different discharge current densities (i.e., from 50 to 800 μA/cm^2). The photo charge process proceeded for 5 s, during which the voltage of the power pack rapidly increased to 1 V under light illumination and remained stable, signifying the efficient charge transfer from PSC to supercapacitor and excellent electrical conductivity of Ti substrate and acid-treated TiO_2 electrode. The areal capacitances were calculated according to the discharge curves (Figure 4b), which were in good agreement with the results obtained in the galvanostatic charge/discharge mode (Figure 3b). The energy density of the supercapacitor with photo charge was calculated to be 0.40 μWh/cm^2 at the discharge current density of 100 μA/cm^2 (see eqs 1−2 in Experimental Section; Figure S8). Consequently, the overall photoelectric conversion and storage efficiency ($\eta_{overall}$) in the integrated power pack was determined to be 9.18% based on eqs 2−5, yielding an energy storage efficiency of 68.66% according to eq 6. Notably, the $\eta_{overall}$ obtained in this work is remarkable among reported integrated PSCs and supercapacitors (Table S1). The stability of the integrated power pack was examined via photo charge and galvanostatic discharge at the current density of 400 μA/cm^2. Specifically, the slight increase of the capacitance during the initial 10 cycles could be attributed to the surface wetting-induced activation process of the electrode.[23] The discharge areal capacitance retained 99% of its initial value after 100 cycles (Figure 4c), suggesting the superior stability of the as-crafted monolithic perovskite solar capacitor.

In summary, we demonstrated the assembly of a high-performance solar power pack via integrating PSC and supercapacitor into a single, intimately connected device (i.e., monolithic perovskite solar capacitor) enabled by employing double-sided TiO_2 nanotube arrays on Ti foil as electrode. In contrast to the two respective subcells (i.e., PSC and supercapacitor) that utilize a pristine TiO_2 nanotube array electrode, their performance is greatly improved concurrently through increasing the conductivity of the TiO_2 nanotube arrays facilitated by acid treatment followed by O_2 plasma exposure on one side of double-sided TiO_2 nanotube arrays for the PSC subcell and by acid treatment only on the other side of double-sided TiO_2 nanotube arrays for the supercapacitor subcell. Benefiting from efficient charge transfer between the two TiO_2 nanotube arrays bound through highly conductive Ti foil, the hybrid power pack delivers a high overall optoelectrical energy conversion and storage efficiency of 9.18% with fast response and excellent cycling capability. Such a monolithic perovskite solar capacitor manifests a set of intriguing characteristics, including a highly compact structure, facile fabrication, low weight, and outstanding stability. Soft integrated solar energy conversion and storage systems of

https://doi.org/10.1021/acsenergylett.2c00090
ACS Energy Lett. 2022, 7, 1260−1265

interest may also be feasible by leveraging the flexible nature of the thin Ti foil.

■ ASSOCIATED CONTENT

Supporting Information

The Supporting Information is available free of charge at https://pubs.acs.org/doi/10.1021/acsenergylett.2c00090.

Experimental section, transmittance spectra, linear sweep voltammetry curves, SEM images of TiO_2 nanotubes, photovoltaic performance statistics, and energy densities (PDF)

■ AUTHOR INFORMATION

Corresponding Author

Zhiqun Lin − *School of Materials Science and Engineering, Georgia Institute of Technology, Atlanta, Georgia 30332, United States;* orcid.org/0000-0003-3158-9340; Email: zhiqun.lin@mse.gatech.edu

Author

Meng Zhang − *School of Materials Science and Engineering, Georgia Institute of Technology, Atlanta, Georgia 30332, United States*

Complete contact information is available at: https://pubs.acs.org/10.1021/acsenergylett.2c00090

Notes

The authors declare no competing financial interest.

■ ACKNOWLEDGMENTS

The work is supported by the National Science Foundation (ECCS 1914562).

■ REFERENCES

(1) K, N.; Rout, C. S. Photo-Powered Integrated Supercapacitors: A Review on Recent Developments, Challenges and Future Perspectives. *J. Mater. Chem. A* **2021**, *9*, 8248−8278.

(2) Devadiga, D.; Selvakumar, M.; Shetty, P.; Santosh, M. Recent Progress in Dye Sensitized Solar Cell Materials and Photo-Supercapacitors: A Review. *J. Power Sources* **2021**, *493*, 229698.

(3) Zhang, M.; Cui, X.; Wang, Y.; Wang, B.; Ye, M.; Wang, W.; Ma, C.; Lin, Z. Simple Route to Interconnected, Hierarchically Structured, Porous Zn2sno4 Nanospheres as Electron Transport Layer for Efficient Perovskite Solar Cells. *Nano Energy* **2020**, *71*, 104620.

(4) Zhang, M.; Ye, M.; Wang, W.; Ma, C.; Wang, S.; Liu, Q.; Lian, T.; Huang, J.; Lin, Z. Synergistic Cascade Carrier Extraction Via Dual Interfacial Positioning of Ambipolar Black Phosphorene for High-Efficiency Perovskite Solar Cells. *Adv. Mater.* **2020**, *32*, 2000999.

(5) Liu, F.; Wang, M.; Liu, X.; Wang, B.; Li, C.; Liu, C.; Lin, Z.; Huang, F. A Rapid and Robust Light-and-Solution-Triggered in Situ Crafting of Organic Passivating Membrane over Metal Halide Perovskites for Markedly Improved Stability and Photocatalysis. *Nano Lett.* **2021**, *21*, 1643−1650.

(6) Wang, B.; Li, H.; Dai, Q.; Zhang, M.; Zou, Z.; Brédas, J. L.; Lin, Z. Robust Molecular Dipole-Enabled Defect Passivation and Control of Energy-Level Alignment for High-Efficiency Perovskite Solar Cells. *Angew. Chem., Int. Ed.* **2021**, *60*, 17664−17670.

(7) NREL. Best Research-Cell Efficiency Chart. https://www.nrel.gov/pv/cell-efficiency.html (accessed 2022-02-30).

(8) Xu, X.; Li, S.; Zhang, H.; Shen, Y.; Zakeeruddin, S. M.; Graetzel, M.; Cheng, Y.-B.; Wang, M. A Power Pack Based on Organometallic Perovskite Solar Cell and Supercapacitor. *ACS Nano* **2015**, *9*, 1782−1787.

(9) Du, P.; Hu, X.; Yi, C.; Liu, H. C.; Liu, P.; Zhang, H. L.; Gong, X. Self-Powered Electronics by Integration of Flexible Solid-State Graphene-Based Supercapacitors with High Performance Perovskite Hybrid Solar Cells. *Adv. Funct. Mater.* **2015**, *25*, 2420−2427.

(10) Xu, J.; Ku, Z.; Zhang, Y.; Chao, D.; Fan, H. J. Integrated Photo-Supercapacitor Based on Pedot Modified Printable Perovskite Solar Cell. *Adv. Mater. Technol.* **2016**, *1*, 1600074.

(11) Liu, Z.; Zhong, Y.; Sun, B.; Liu, X.; Han, J.; Shi, T.; Tang, Z.; Liao, G. Novel Integration of Perovskite Solar Cell and Supercapacitor Based on Carbon Electrode for Hybridizing Energy Conversion and Storage. *ACS Appl. Mater. interfaces* **2017**, *9*, 22361−22368.

(12) Liang, J.; Zhu, G.; Lu, Z.; Zhao, P.; Wang, C.; Ma, Y.; Xu, Z.; Wang, Y.; Hu, Y.; Ma, L.; et al. Integrated Perovskite Solar Capacitors with High Energy Conversion Efficiency and Fast Photo-Charging Rate. *J. Mater. Chem. A* **2018**, *6*, 2047−2052.

(13) Liang, J.; Zhu, G.; Wang, C.; Zhao, P.; Wang, Y.; Hu, Y.; Ma, L.; Tie, Z.; Liu, J.; Jin, Z. An All-Inorganic Perovskite Solar Capacitor for Efficient and Stable Spontaneous Photocharging. *Nano Energy* **2018**, *52*, 239−245.

(14) Zhu, T.; Yang, Y.; Liu, Y.; Lopez-Hallman, R.; Ma, Z.; Liu, L.; Gong, X. Wireless Portable Light-Weight Self-Charging Power Packs by Perovskite-Organic Tandem Solar Cells Integrated with Solid-State Asymmetric Supercapacitors. *Nano Energy* **2020**, *78*, 105397.

(15) Ge, M.; Cao, C.; Huang, J.; Li, S.; Chen, Z.; Zhang, K.-Q.; Al-Deyab, S.; Lai, Y. A Review of One-Dimensional Tio 2 Nanostructured Materials for Environmental and Energy Applications. *J. Mater. Chem. A* **2016**, *4*, 6772−6801.

(16) Zhang, M.; Xuan, X.; Wang, W.; Ma, C.; Lin, Z. Anode Photovoltage Compensation-Enabled Synergistic Co2 Photoelectrocatalytic Reduction on a Flower-Like Graphene-Decorated Cu Foam Cathode. *Adv. Funct. Mater.* **2020**, *30*, 2005983.

(17) Wang, B.; Biesold, G. M.; Zhang, M.; Lin, Z. Amorphous Inorganic Semiconductors for the Development of Solar Cell, Photoelectrocatalytic and Photocatalytic Applications. *Chem. Soc. Rev.* **2021**, *50*, 6914−6949.

(18) Wang, B.; Zhang, M.; Cui, X.; Wang, Z.; Rager, M.; Yang, Y.; Zou, Z.; Wang, Z. L.; Lin, Z. Unconventional Route to Oxygen-Vacancy-Enabled Highly Efficient Electron Extraction and Transport in Perovskite Solar Cells. *Angew. Chem., Int. Ed.* **2020**, *59*, 1611−1618.

(19) Lu, X.; Wang, G.; Zhai, T.; Yu, M.; Gan, J.; Tong, Y.; Li, Y. Hydrogenated Tio2 Nanotube Arrays for Supercapacitors. *Nano Lett.* **2012**, *12*, 1690−1696.

(20) Yu, J.; Zhao, X. Effect of Surface Treatment on the Photocatalytic Activity and Hydrophilic Property of the Sol-Gel Derived Tio2 Thin Films. *Mater. Res. Bull.* **2001**, *36*, 97−107.

(21) Wang, G.; Wang, H.; Ling, Y.; Tang, Y.; Yang, X.; Fitzmorris, R. C.; Wang, C.; Zhang, J. Z.; Li, Y. Hydrogen-Treated Tio2 Nanowire Arrays for Photoelectrochemical Water Splitting. *Nano Lett.* **2011**, *11*, 3026−3033.

(22) Zhou, H.; Zhang, Y. Electrochemically Self-Doped Tio2 Nanotube Arrays for Supercapacitors. *J. Phys. Chem. C* **2014**, *118*, 5626−5636.

(23) Moosavifard, S. E.; El-Kady, M. F.; Rahmanifar, M. S.; Kaner, R. B.; Mousavi, M. F. Designing 3d Highly Ordered Nanoporous Cuo Electrodes for High-Performance Asymmetric Supercapacitors. *ACS Appl. Mater. Interfaces* **2015**, *7*, 4851−4860.